Naval Research Laboratory

Washington, DC 20375-5000

NRL Memorandum Report 6704

AD-A226 552

A Study of Confined Diffusion Flames

J. L. ELLZEY,* K. J. LASKEY,** AND E. S. ORAN

Laboratory for Computational Physics and Fluid Dynamics

**Berkeley Research Associates*
Springfield, VA

***Grumman Space Station Program Support Division*
Reston, VA

DTIC
ELECTE
SEP 17 1990
S D

September 4, 1990

Approved for public release; distribution unlimited.

REPORT DOCUMENTATION PAGE

Form Approved
OMB No. 0704-0188

Public reporting burden for this collection of information is estimated to average 1 hour per response, including the time for reviewing instructions, searching existing data sources, gathering and maintaining the data needed, and completing and reviewing the collection of information. Send comments regarding this burden estimate or any other aspect of this collection of information, including suggestions for reducing this burden, to Washington Headquarters Services, Directorate for Information Operations and Reports, 1215 Jefferson Davis Highway, Suite 1204, Arlington, VA 22202-4302, and to the Office of Management and Budget, Paperwork Reduction Project (0704-0188), Washington, DC 20503.

1. AGENCY USE ONLY (Leave blank)	2. REPORT DATE	3. REPORT TYPE AND DATES COVERED
	1990 September 4	

4. TITLE AND SUBTITLE

A Study of Confined Diffusion Flames

5. FUNDING NUMBERS

PE - 61153N
PR - 0N280-071
TA - 0110943
WU - 44153000

6. AUTHOR(S)

J. L. Ellzey, K. J. Laskey and E. S. Oran

7. PERFORMING ORGANIZATION NAME(S) AND ADDRESS(ES)

Naval Research Laboratory
Washington, DC 20375-5000

8. PERFORMING ORGANIZATION REPORT NUMBER

NRL Memorandum Report 6704

9. SPONSORING/MONITORING AGENCY NAME(S) AND ADDRESS(ES)

Office of Naval Research
800 N. Quincy Street
Arlington, VA 22217-5000

10. SPONSORING/MONITORING AGENCY REPORT NUMBER

11. SUPPLEMENTARY NOTES

* Berkeley Research Associates, Springfield, VA
** Grumman Space Station Program Support Division, Reston, VA

12a. DISTRIBUTION/AVAILABILITY STATEMENT

Approved for public release; distribution unlimited.

12b. DISTRIBUTION CODE

13. ABSTRACT *(Maximum 200 words)*

A numerical simulation of an axisymmetric confined diffusion flame formed between a $H_2 - N_2$ jet and coflowing air at 30 cm/s is presented in this paper. For the initial computations, the restrictions of the Burke-Schumann theory are imposed and the results of the computation are compared with the analytical solution for flame location. For both the underventilated and overventilated flames, the results of the computations are in excellent agreement with the analytical solution. However, the flame behavior becomes more complex as the restructions are relaxed. When variable diffusion coefficients and densities are included in the calculation, small radial velocities are induced and the flame interface is slightly distorted. When heat release is included, the flame is shorter and an unsteady mixing region forms at the fuel-oxidizer interface. The instabilities are damped when viscous effects are included. Large-scale instabilities form in the oxidizer region with a frequency of approximately 15-20 Hz when gravity is included in the calculation.

14. SUBJECT TERMS			15. NUMBER OF PAGES 31
			16. PRICE CODE
17. SECURITY CLASSIFICATION OF REPORT	18. SECURITY CLASSIFICATION OF THIS PAGE	19. SECURITY CLASSIFICATION OF ABSTRACT	20. LIMITATION OF ABSTRACT
UNCLASSIFIED	UNCLASSIFIED	UNCLASSIFIED	UL

NSN 7540-01-280-5500

Standard Form 298 (Rev 2-89)
Prescribed by ANSI Std 239-18
298-102

CONTENTS

DTIC COPY INSPECTED 1

Accession For
NTIS GRA&I
DTIC TAB
Unannounced
Justification
By
Distribution/
Availability Codes
Dist | Avail and/or Special
A-1

A STUDY OF CONFINED DIFFUSION FLAMES

I. Introduction

The analytical work of Burke and Schumann (1) has formed many of our fundamental ideas about laminar diffusion flames. In the original Burke-Schumann problem, axisymmetric coflowing streams of fuel and oxidizer flow through a confined duct, and the velocities, densities, and diffusion coefficients of the fuel and oxidizer are equal. Reaction is instantaneous, resulting in a flame sheet of infinitesimal thickness in which the reaction rate is effectively controlled by the diffusion rate. The solution to this problem is an equation which can be solved for the location of the flame front. In the original analysis, Burke and Schumann chose the diffusion coefficients in order to obtain good agreement with experiments. Later work (2) extended the theory to describe the flame interface for unequal velocities and diffusion coefficients. Further extensions of the theory predict the behavior of multiple, coupled diffusion flames (3,4).

Many of the restrictive assumptions in the Burke-Schumann analysis can be removed by a numerical solution of the reactive flow equations. In particular, there are a number of steady-state numerical solutions that simulate laminar diffusion flames. Gosman et al. (5) solved the two-dimensional steady-state equations for a case in which all of the diffusion coefficients were the same and the Lewis number was unity. Mitchell et al. (6) numerically simulated steady-state flames with nonunity Lewis numbers but kept the basic idea of the flame sheet model.

This paper describes a time-dependent, axisymmetric, compressible numerical model which is designed specifically to simulate the nonsteady behavior of diffusion flames. It contains submodels for finite-rate chemistry, viscosity, thermal conduction, and the temperature dependence of material properties such as specific heats and diffusion coefficients. As one of the

Manuscript approved June 5, 1990.

first uses of the diffusion flame model, we simulate a Burke-Schumann flame and remove the restrictions individually. We present results for a classic Burke-Schumann flame with all of the restrictions included in the analysis and compare to the anlytical solution. Then we include the following sequentially:

1. Variable density and diffusion coefficients, radial convection, and axial diffusion,
2. Heat release,
3. Viscous effects,
4. Gravitational effects.

This set of computations is a benchmark of the model that is currently being applied to more complex transitional diffusion flames. Although practical examples of Burke-Schumann flames are not as abundant as turbulent or unsteady flames, they represent an important class of problems which can be studied through theory, computation, and experiment.

Besides the applications of the model to the Burke-Schumann problem, this paper also describes the numerical model in detail. Specific notable features of the model are its time dependence, the finite-rate chemical model, the temperature dependence of the transport coefficients, and the nonunity Lewis number. The new elements of the numerical model that make such computations possible are the BIC-FCT algorithm used to compute the convection and the parametric diffusion-reaction (PDR) model used for the finite-rate chemistry. These features and algorithms are described in some detail in the next section of this paper.

II. Numerical Methods and the Model Structure

The numerical model used for this study is based on those originally developed by Patnaik et al. (7) to simulate low-speed premixed flames and by Laskey (8) to simulate jet flames . The program solves the equations

for conservation of mass density, momentum, energy, and individual species number densities:

$$\frac{\partial \rho}{\partial t} + \nabla \cdot (\rho \mathbf{v}) = 0 \tag{1}$$

$$\frac{\partial \rho \mathbf{v}}{\partial t} + \nabla \cdot (\rho \mathbf{v}\mathbf{v}) = -\nabla P - \rho \mathbf{G} - \nabla \cdot \tau \tag{2}$$

$$\frac{\partial E}{\partial t} + \nabla \cdot (E\mathbf{v}) = -\nabla \cdot P\mathbf{v} + \nabla \cdot (\kappa \nabla T) - \nabla \cdot \sum_{k=1}^{n_{sp}} n_k \mathbf{v}_k h_k + Q \tag{3}$$

$$\frac{\partial n_k}{\partial t} + \nabla \cdot (n_k \mathbf{v}) = -\nabla \cdot (n_k \mathbf{v}_k) + w_k \ , \tag{4}$$

with the additional relations

$$P_k = n_k k T \ , \tag{5}$$

and

$$d\epsilon = \rho c_v \, dT \ . \tag{6}$$

The various quantites used in these equations and throughout this article are defined in the accompanying Nomenclature.

Equations (1) – (4) contain terms representing convection, thermal conduction, species diffusion, chemical reactions, and viscosity. These equations are then rewritten in terms of finite-difference approximations on an Eulerian mesh and solved numerically for specified boundary and initial conditions. The accuracy of the solution is determined by the specific finite-difference algorithm, the spatial resolution set by the computational grid, and the temporal resolution set by the timestep. There is a wide range of important spatial and temporal scales in reacting flow problems. Because it is not usually possible to resolve phenomena on all of these scales, the smallest scales must be modeled phenomenologically.

However, as computational capabilities and model inputs improve, it should be possible to replace certain submodels by more accurate or faster submodels. For example, assuming that rate of diffusion is much less than the reaction rate helps justify using a global reaction mechanism. Using such a global reaction is, however, approximate and we believe that within a

few years it will be possible to include a detailed set of elementary reaction rates. Therefore, the computer program is designed in a modular form so that particular submodels can be updated in a relatively straightforward way. In the computer program, algorithms representing different physical processes are solved separately and then the results are combined, as summarized below. More detailed descriptions are presented by Laskey (8).

Convection

The solution to the convective terms in Eqs. (1) – (4) is obtained using the new algorithm, Barely Implicit Correction to Flux-Corrected Transport (BIC-FCT) that was developed to solve the convection equations for low-velocity flows (9). The Flux-Corrected Transport algorithm itself is an explicit, finite-difference algorithm that is constructed to have fourth-order phase accuracy (10). Through a two-step predictor-corrector algorithm, FCT ensures that all conserved quantities remain monotone and positive. The FCT procedure is to first modify the properties of a high-order algorithm by adding diffusion during a convection step and then to subtract out the diffusion in an antidiffusion phase. In addition, fluxes are limited to ensure that no new unphysical maxima or minima are added during the convection process.

However, because FCT is an explicit algorithm, the numerical timestep required for accuracy and stability is limited by the velocity of sound according to the Courant-Friedrichs-Lewy condition, $\Delta t < min(\Delta x/c_s)$. To avoid this restriction, which would make computations of slowly evolving flows prohibitively expensive, the convection equations are usually solved implicitly. This filters out the sound waves from the equation and, therefore, removes the sound-speed condition. Patnaik et al. (7) developed BIC-FCT so that the timestep would be limited by the fluid velocity and not the sound speed. This implementation has great advantages for computations of slow flows because one BIC-FCT timestep costs the same as one regular FCT explicit timestep, but the size of the timestep might be a factor of 50 to 100 times greater.

BIC-FCT is based on the idea proposed by Casulli and Greenspan (11) that only the terms containing the pressure in the momentum equation and the velocity in the energy equation must be treated implicitly in order to avoid the sound-speed limitation on the timestep. BIC-FCT has three steps. In the first step, the conservation equations are solved explicitly with FCT using a relatively large timestep governed by fluid velocity. In the second step, the energy and momentum equations are rewritten in terms of a pressure correction, δp. These equations can be manipulated such that only one elliptic equation for δp must be solved. In the third step, final values of momenta and energy are obtained by adding the pressure correction terms. Patnaik et al. (7) have used this algorithm in a two-dimensional flame program to investigate laminar instabilities in premixed flames.

The form used for the relation between the change in internal energy and the change in the pressure, required in the second step of BIC-FCT, can be derived from Eq. 6 and simplifies under certain assumptions (8). For example, if all of the constituents have the same temperature dependence, we can write

$$d\epsilon = \frac{\delta p}{\gamma_m - 1} + \left(\epsilon - \frac{p}{\gamma_m - 1}\right) d(\ln n) , \qquad (7)$$

where γ_m is a mixture quantity. The second term in Equation (7) is dependent on the change in the local species concentration and is important only in the reaction zone. In our simplified reaction submodel, we do not include the intermediate species. Consequently, this term cannot be represented accurately and we do not include it explicitly. In the reaction zone, we are primarily interested in representing a finite flame thickness and reproducing the correct maximum temperature. We calibrate the reaction submodel to predict a realistic flame temperature and flame thickness without this term included.

Molecular Diffusion

An algorithm for molecular diffusion has been formulated to estimate the molecular diffusion fluxes without having to solve a full matrix problem.

The change in species concentration for each species k due to molecular diffusion is

$$\frac{\partial n_k}{\partial t} = -\nabla \cdot n_k \mathbf{v}_k \tag{8}$$

where the diffusion velocity, $\mathbf{v}_k$, is calculated from Fick's Law,

$$\mathbf{v}_k = -\frac{1}{X_k} D_{km} \nabla X_k \tag{9}$$

and then corrected by a procedure described by Kee et al. (12) to satisfy the requirement that the sum of the diffusion fluxes is zero. This method is algebraically equivalent to the first iteration of the DFLUX algorithm (13), an iterative approach that solves for diffusion velocities to optional accuracy.

The change in total energy density due to molecular diffusion alone is

$$\frac{\partial E}{\partial t} = -\nabla \cdot \sum_{k=1}^{n_{sp}} n_k h_k \mathbf{v}_k \ . \tag{10}$$

This energy term is calculated during the diffusion algorithm but is added to the total energy at the end of the time step.

The explicit finite-differencing procedure applied to this term introduces a numerical stability condition,

$$D_{km} \Delta t \left(\frac{1}{\Delta x^2} + \frac{1}{\Delta y^2} \right) < \frac{1}{2} \ , \tag{11}$$

where D_{km} is the diffusion coefficient for species k diffusing into a mixture. To maintain stability, this condition may require a timestep smaller than that required by the convection, which adds substantially to the cost of the calculation. To avoid this problem, the diffusion term is evaluated several times during a convection timestep. This is especially important if the elevated temperature of the reacting flow results in higher diffusion coefficients.

Binary diffusion coefficients are calculated from kinetic theory and are in the following form

$$D_{kl} = \frac{A_{kl}}{n} T^{B_{kl}} \ , \tag{12}$$

where A_{kl} and B_{kl} depend on species k and l. Values for A_{kl} and B_{kl} have been tabulated by Kailasanath et al. (14). The diffusion coefficient of species k in a mixture of n_{sp} species is calculated according to

$$D_{km} = \frac{1 - Y_k}{\sum_{\substack{kk=1 \\ kk \neq k}}^{n_{sp}} \frac{X_{kk}}{D_{k,l}}} \tag{13}$$

where Y_k is the mass fraction of species k, X_k is the mole fraction of species k, and $D_{k,l}$ is the diffusion coefficient of species k diffusing into species l (15).

Thermal Conduction

A two-dimensional model has also been formulated to simulate thermal conduction. Restricting our attention only to the Fourier conduction term, the energy equation appears as

$$\frac{\partial E}{\partial t} = -\nabla \cdot (\kappa \nabla T) \, . \tag{14}$$

As with the molecular diffusion algorithm, the use of explicit finite differencing introduces a stability limit for the thermal conduction calculation,

$$\frac{\kappa \Delta t}{\rho c_p} \left(\frac{1}{\Delta x^2} + \frac{1}{\Delta y^2} \right) < \frac{1}{2} \, , \tag{15}$$

where $\kappa / \rho c_p$ is the thermal diffusivity. The thermal conduction term is evaluated several times during each convection time step in the same manner as the molecular diffusion term. Thermal conductivities, κ_k, for the individual species were calculated from kinetic theory over the temperature range 300 K to 3300 K, and these values were fit to a third-order polynomial. The mixture thermal conductivity is then calculated using the expression from Kee et al. (12)

$$\kappa = \frac{1}{2} \left[\sum_{k=1}^{n_{sp}} X_k \kappa_k + \frac{1}{\sum_{k=1}^{n_{sp}} \frac{X_k}{\kappa_k}} \right] \, . \tag{16}$$

Viscous Stress

The momentum transport associated with viscous diffusion only is

$$\frac{\partial \rho \mathbf{v}}{\partial t} = -\nabla \cdot \tau \tag{17}$$

where

$$\tau = \left(\frac{2}{3}\mu - \zeta\right)(\nabla \cdot \mathbf{v})\mathbf{I} - \mu\left[(\nabla \mathbf{v}) + (\nabla \mathbf{v})^T\right] \tag{18}$$

and ζ is the second coefficient of viscosity and is assumed to equal zero. Equation 17 is rewritten in terms of an explicit finite difference approximation which introduces a numerical stability condition,

$$\frac{\mu \Delta t}{\rho}\left(\frac{1}{\Delta x^2} + \frac{1}{\Delta y^2}\right) < \frac{1}{2}\,. \tag{19}$$

The values for μ_k were calculated from kinetic theory over the temperature range 300 K to 3000 K and fit to a third-order polynomial. The mixture viscosity was calculated from

$$\mu = \sum_{k=1}^{n_{sp}} \frac{X_k \mu_k}{\sum_{j=1}^{n_{sp}} X_j \Phi_{kj}} \tag{20}$$

where Φ_{kj} is a weighting factor

$$\Phi_{kj} = \frac{1}{\sqrt{8}}\left(1 + \frac{M_k}{M_j}\right)^{-\frac{1}{2}}\left(1 + \left(\frac{\mu_k}{\mu_j}\right)^{\frac{1}{2}}\left(\frac{M_j}{M_k}\right)^{\frac{1}{4}}\right)^2 \tag{21}$$

and M_k is the molecular weight of species k (16).

Model for Chemical Reactions

Ideally, we would like to simulate the chemical reaction by including a detailed set of elementary reactions to describe the production of the individual species and the energy release in the flame. However, the cost of

computer time and memory makes this prohibitive for problems in which the flows are complex. We have, therefore, used the parametric diffusion-reaction (PDR) model that reflects many of the major characteristics of a more detailed calculation.

In the original flame-sheet model proposed by Burke and Schumann (1), the fuel and oxidizer react completely and are not permitted to coexist. Thus, the flame is an infinitesimal interface between regions of fuel and oxidizer. In the PDR model developed by Laskey (8), a single global reaction mechanism, $2H_2 + O_2 \rightarrow 2H_2O$, is used but the fuel and oxidizer do not react instantaneously. Instead, the reaction occurs over a finite time interval.

In a real flame, the increase in temperature in the reaction zone is a result of the change in internal energy of the local mixture which includes reactants, product, and intermediates. In our simulation, we do not include the intermediates and, as a result, the specific heat of the gas is not represented accurately in the flame zone. Even if we obtain a realistic overall rate for the global reaction, the temperature in the flame zone is too high unless we compensate for the inaccuracy in the specific heat.

The two important physical characteristics of the flame zone are the maximum temperature and thickness. We calibrated the reaction rate in a one-dimensional transient diffusion flame such that a thin reaction zone developed and adjusted the heat of formation such that the maximum temperture was approximately the adiabatic flame temperature for a stoichiometric mixture of fuel and oxidizer.

Coupling

A complete solution to the governing equations requires solving the terms for individual processes as well as accounting for the interaction among the processes. In the calculations presented below, we use timestep splitting, which assumes that the net effect of all the processes is the sum of the solutions to individual processes. This technique is valid if the changes in the dependent variables during a timestep are small. Table 1 is an outline that shows the order of the computations during one timestep in the computer code.

Table 1. Outline of Diffusion Flame Code

Initialize Variables
* Increment time
1. Thermal Conduction
    Integrate from t to $t + \Delta t$:
    Calculate $\Delta\epsilon_1$
    Do not update any variables
    (Subcycle as necessary)
2. Ordinary Diffusion
    Integrate from t to $t + \Delta t$:
    Only update $\{n_i(x)\}$
    Calculate $\Delta\epsilon_2$
    (Subcycle as necessary)
3. Viscosity
    Integrate from t to $t + \Delta t$:
    Only update $\rho\mathbf{v}$
    Calculate $\Delta\epsilon_3$
4. Chemical Reactions
    Integrate from t to $t + \Delta t$:
    Only update $\{n_i(x)\}$
    Calculate $\Delta\epsilon_4$
5. Convective Transport
    Integrate from t to $t + \Delta t$:
    x direction transport
        Update $\rho, \rho\mathbf{v}, E, n_i$
    y direction transport
        Update $\rho, \rho\mathbf{v}, E, n_i$
    Implicit correction– update p, ϵ, and E
Start New Timestep (go to * above)

Due to different requirements of accuracy and stability, the type of coupling used for lower velocity implicit calculations is different from that needed for higher velocity explicit calculations. General information on these approaches is described in some detail in Reference (10), Chapter 13. In these implicit computations, the changes in pressure or internal energy resulting from the individual processes should not be added into the solution as soon

as they are computed, but instead should be accumulated over the timestep. The entire change in internal energy is then included in the fluid convection step. The specific coupling technique used in this program (17) allows larger changes in variables per timestep while maintaining numerical stability.

III. Application of the Algorithm to a Confined Diffusion Flame

The numerical procedure described above was used to simulate several confined diffusion flames. The geometry used in the calculations (Figure 1) consists of a an inner jet of radius a and an outer annular region between the jet and the walls at radius b. Typically, fuel flows through the inner jet and oxidizer flows through the outer annular region. The appropriate boundary conditions for this geometry are

1. $r = 0$ is a line of symmetry,
2. $r = b$ is a solid, adiabatic, free-slip wall,
3. $z = 0$ is an inflow boundary where the concentrations, velocities, and temperatures of the fuel, oxidizer, and inert are specified,
4. $z = z_1$ is an outflow boundary where the pressure is adjusted to equal 1 atmosphere.

For the Burke-Schumann flame, $a = 1$, $b = 2$, $z_1 = 10$ cm. The computational domain consists of a 32×88 grid. The grid spacing is uniform in the radial and the axial directions. Calculations on finer grids, such as 64×176, resulted in smoother flame interfaces but did not change the result significantly. The computational time step is 1 ms.

For the simulations of a confined diffusion flame without all of the Burke-Schumann restrictions, $a = 0.5$, $b = 2.5$, $z_1 = 10$ cm. The grid consisted of 64×88 cells with fine cells concentrated around the jet exit. In the radial direction, the grid spacing is approximately 0.02 cm from the centerline to $r = 0.7$ cm and then expands gradually to a grid spacing of 0.12 at $r = 2.5$ cm. In the axial direction, the grid spacing is uniform through the domain and equals 0.11 cm. A typical timestep is 10 μs.

Computational Time Requirements

A two-dimensional simulation, which includes convection, chemical reaction, molecular diffusion, viscous diffusion, and conduction, requires approximately 25 μs per grid point per timestep on a Cray Y-MP. The convection algorithm requires approximately twice the cpu time of either the molecular diffusion or the viscous diffusion algorithms and four times that of the conduction algorithm. The parametric diffusion-reaction flame model requires insignificant cpu time.

IV. The Burke-Schumann Flame

Burke and Schumann (1) found a solution for a set of equations that give the location of the flame interface for a laminar diffusion flame under a certain set of limiting conditions. The Burke-Schumann analysis of the laminar diffusion flame and a comparison of their analysis to the computatuional results are presented in this section.

In order to solve the equations, Burke and Schumann invoked a number of simplifying assumptions:

1. The velocities of the fuel and oxidizer are equal and uniform everywhere,
2. The radial velocity is zero,
3. The densities and diffusion coefficients are equal for all components,
4. Radial diffusion is much greater than axial diffusion,
5. Reaction takes place at an infinitesimal flame sheet.

With these assumptions, the conservations equations can be reduced to a single species equation which is solved with the following boundary conditions:

1. $r = b$ is a solid wall,
2. $r = 0$ is a line of symmetry,
3. At $z = 0$, the compositions of the fuel and oxidizer streams are specified.

The analytic solution to the equation yields the location of the flame surface as a function of a/b and the initial concentrations of fuel and oxidizer.

These assumptions enforce various unrealistic restrictions on the flow field. If the velocity is uniform across the radius of the tube, then the no-slip condition cannot be imposed at the wall boundary and, as a result, a parabolic velocity profile typical of confined flows cannot develop. The assumption of equal densities requires that one mole of fuel reacts with s moles of oxidizer to form $1 + s$ moles of product. Finally, in a real flame, the volumetric expansion associated with heat release distorts the one-dimensional flow resulting in a radial component to the velocity and a nonuniform density field. Consequently, the heat release and expansion are not considered in the Burke-Schumann analysis.

Figure 1 shows two general cases that can be solved with the Burke-Schumann approach: the underventilated flame, which has insufficient oxidizer for complete burning, and the overventilated flame, which has excess oxidizer. In the overventilated case, the fuel is completely consumed in the reaction and the flame surface is closed at the centerline of the jet. In the underventilated case, the flame surface bends outward and is attached to the outer wall. The two different cases may be obtained by changing either the ratio a/b or the composition of the fuel or oxidizer stream.

While the details of most flames cannot be represented realistically by the results of the Burke-Schumann analysis, the predictions of the analysis are surprisingly good for steady, laminar flames. In addition, it provides an analytical result against which to test the numerical model.

Simulation of the Burke-Schumann Flame

For the first cases considered in this study, the ratio of the radii, a/b, is 0.5 ($a = 1$ cm, $b = 2$ cm), and the fuel flows in the inside jet and oxidizer flows in the outside annular region. The velocities of the fuel and oxidizer streams are uniform and equal to 10 cm/s. The densities of the two streams are equal but the composition was varied by diluting the fuel or oxidizer stream with an inert gas. All diffusion coefficients were equal to an equivalent mixture of H_2 and N_2 diffusing into O_2.

Figure 2 shows a sequence of fuel and oxidizer concentration contours for the numerical simulation of the Burke-Schumann flame as it evolves from the initial condition to a steady state. At $t = 0$, pure fuel exists at $r < 1$ cm and an oxidizer mixture, consisting of one part oxidizer and one part inert, exists at $r > 1$ cm. Since there is an overall excess of oxidizer, the fuel and oxidizer interface moves inward during time steps 0 to 1000 because the fuel is completely consumed in the reaction at the flame surface. In all cases, fuel and oxidizer do not coexist because the Burke-Schumann flame sheet model assumes that the reaction goes to completion. At time step 1000 which equals 1 second of physical time, the concentration field has reached a steady state.

In Figure 3a, the computed contours for 1% of the inlet fuel concentration and 1% of the inlet oxidizer concentration are superimposed on the Burke-Schumann solution for the flame front. The analytic solution is the interface between the fuel and oxidizer regions and should correspond to the zeroth contour for either the fuel or the oxidizer, and it should occur between the two 1% contours. Figure 3b shows a similar calculation for a fuel mixture of one part fuel and three parts by volume of inert reacting with pure oxidizer. In both cases, the computed flame front is within one cell of the analytical solution.

A similar computation was conducted for an underventilated Burke-Schumann flame. In this case, the inlet jet was pure fuel and the oxidizer consisted of one part of oxidizer to four parts inert. The steady state fuel contours are shown in Figure 3c with the analytic solution superimposed. In this case, the flame bends outward and attaches to the outer wall. Again, the flame shape and height are within the accuracy of the calculation.

V. Elimination of the Burke-Schumann Restrictions

The restrictions on the Burke-Schumann analysis prevent its application to a wide range of problems. In this section, we describe how the computed results are affected by eliminating some of the restrictions in the analysis.

In these computations, the ratio of the inner to the outer radii is 0.2 (a = 0.5, b = 2.5) and the inlet velocity is 30 cm/s. The fuel consists of 3.41 parts of H_2 to 1 part N_2 by volume and the oxidizer is air.

Introduction of correct stoichiometry, densities, and diffusion coefficients, but maintaining the conditions of uniform inlet velocity and isothermal reaction, required that radial gradients be included. The full system of equations (1) - (4) were solved for this case and the results are shown in Figure 4 after 0.4 s. Figures 4a and 4b show the axial and radial velocity contours and Figures 4c and 4d show the contours of fuel and oxidizer mole fractions. Small radial velocities are induced in the reaction zone even though heat release is not included. The maximum axial velocity of approximately 35 cm/s occurs about 0.25-0.50 cm from the jet centerline. There is a region of lower velocity within the fuel-rich zone close to the centerline which initially consisted of pure fuel mixture. There is only a small region very close to the inlet which is still pure fuel mixture because product has diffused across the jet. This diffusion of heavier gases increases the density in the fuel zone. Because momentum is conserved, the velocity decreases. The flame interface lies between the lowest fuel and oxidizer contours. The flame shape is slightly distorted due to the fluctuations in the radial velocity.

So far, heat release from the chemical reaction has not been included, i.e. Q in Equation (3) is zero. The effects of including heat release are shown in Figure 5 after approximately 0.3 seconds. The volumetric expansion associated with the heat release accelerates the flow resulting in maximum axial velocities of 120 cm/s. The hot gases are accelerated outward in the radial direction with a maximum velocity of about 9 cm/s (Fig. 5d). The radial velocity contours show that the flame is not steady but has vortices which form at the fuel/oxidizer interface. This flame is shorter than that predicted when heat release is not included in the calculation. The increased radial velocity provides an additional mechanism for mixing so the reaction zone is wider and the flame is shorter.

When viscous effects are included in the calculation, the flow field changes again and these results are shown in Figure 6. The gradients in the axial velocity are reduced and the vortical structures are damped. The concentration and temperature fields are similar to those without viscosity. This flame is slightly longer than the flame without viscosity because the radial mixing has been reduced.

In the final simulation, gravitational effects were included. This simulation includes all effects discussed in the equations (1) - (4). This case was started from the flame in Figure 6 and the results after 0.25 seconds are shown in Figure 7. The radial velocity field shows large structures which form in the high temperature region near the jet. These structures convect downstream and change the local concentration field. The H_2 concentration field is not affected by gravity but the O_2 concentration field has changed. Gravity has a significant effect because there is a large density difference between the burnt and unburnt gases in this flow.

Figure 8 shows a time sequence of O_2 mole fraction contours. In the first frame, a bulge appears approximately in the middle of the computational domain and convects upward in frames 2 and 3. By frame 4, the O_2 field is very distorted as the structure convects upward. In the final two frames, the structure continues to roll up as it convects out the computational domain. We estimate the frequency to be 15-20 Hz. These structures are similar to those observed experimentally in unconfined diffusion flames (20-21) and are often attributed to the effect of buoyancy.

VI. Conclusions

The Burke-Schumann analysis has formed many of our ideas about laminar diffusion flames. This simplified approach describes the global nature of a confined laminar flame but ignores many of the physical phenomena in real flames. In this paper, we described a new computer program which includes these effects. The simulations show details of the flames which cannot be observed from the analytical solution.

Introducing variable density and diffusion coefficients for a $H_2 - N_2$ fuel jet with coflowing air results in small radial velocities. In a flame where the inlet fuel and oxidizer velocities are equal, heat release accelerates the gases and produces a mixing region characterized by large-scale instabilities which are damped by viscosity. The effects of heat release and viscosity are not included in the Burke-Schumann analysis but they appear to counter-act each other.

Gravity produces a significant change in the flow field of a confined diffusion flame. The flame fluctuates in time as the bouyancy-driven structures convect upward. These low frequency fluctuations obviously are not represented in the steady state analysis of Burke and Schumann, but these fluctuations do not change the flame location significantly.

Thus, as the Burke-Schumann restrictions are eliminated, the flame characteristics change. Realistic stoichiometry, diffusion coefficients, and densities for a $H_2 - N_2$ flame with coflowing air results in a laminar flame with only small radial velocities. When heat release is included, vortices form in the reaction zone but these structures are damped by viscosity. Finally, gravity induces large-scale structures to form in the region outside of the reaction zone.

Nomenclature

Symbol	Definition
c_s	Speed of sound (cm/s)
c_v	Specific heat (erg/g-K)
D_{ik}	Binary diffusion coefficient between species i and k (cm^2/s)
E	Total energy density (erg/cm^3)
G	Gravitational acceleration constant (980.67 cm/s^2)
h	Enthalpy per molecule (erg/molecule)
$\mathbf{I}$	Unit tensor (nondimensional)
k	Boltzmann constant (1.3805×10^{-16} erg/K)
n	Number density (cm^{-3})
P	Pressure ($dyne/cm^2$)
Q	Energy release rate (erg/cm^3-s^1)
T	Temperature (K)
$\mathbf{v}$	Velocity (cm/s)
w	Production rate ($cm^{-3}s^{-1}$)
x	Spatial coordinate (cm)
X	Mole fraction
y	Spatial coordinate (cm)
Y	Mass fraction
Greek	
ϵ	Specific internal energy (erg/cm^3)
γ	Ratio of specific heats, c_p/c_v
κ	Thermal conductivity coefficient (erg/s-K-cm)
μ	Coefficient of shear viscosity (poise, g/cm-s)
ρ	Mass density (g/cm^3)
τ	Viscous stress tensor ($dynes/cm^2$)
Superscripts	
T	Transpose operation on a matrix
Subscripts	
m	Mixture of species
i, j, k, or l	Individual species

Acknowledgements

This work was sponsored by the Naval Research Laboratory through the Office of Naval Research. The authors would like to thank Dr. Gopal Patnaik for his many helpful suggestions and comments on this work.

References

1. Burke, S.P., and Schumann, T.E.W., *Indust. Eng. Chem.* 20: 998-1004 (1928).
2. Penner, S.S., Bahadori, M.Y. and Kennedy, E.M. *Dynamics of Flames and Reactive System: AIAA Progress in Astronautics and Aeronautics*, J.R. Bowen, N. Manson, A.K. Oppenheim, and R.I. Soloukin (ed.), 95: 261-292 (1984).
3. Bahadori, M. Y., Li, C. -P., and Penner, S.S. in *Dynamics of Flames and Reactive System: AIAA Progress in Astronautics and Aeronautics* (J.R. Bowen, J.-C. Leyer, and R.I. Soloukin, Ed.), 105: 192-206 (1986).
4. Li, C.-P., Wiesenhahn, D., and Penner, S.S., *Combustion and Flame*, 65: 215-225 (1986).
5. Gosman, A.D., Pun, W.M., Runchal, A.K., Spalding, D.B., and Wolfshteim, M., *Heat and Mass Transfer in Recirculating Flows*, Academic Press, London (1969).
6. Mitchell, R.E., Sarofim, A.F., and Clomburg, L.A., *Combustion and Flame* 37: 227-244 (1980).
7. Patnaik, G., Kailasanath, K., Laskey, K.J., and Oran, E.S., *Twenty-Second Symposium (International) on Combustion*, Seattle, WA, Aug. 14-19, 1988, The Combustion Institute, Pittsburgh 1989 p. 1517.
8. Laskey, K. J., *Numerical Study of Diffusion Jet Flames*, Ph.D. dissertation, Department of Mechanical Engineering, Carnegie-Melon University, Pittsburgh, PA (1988).
9. Patnaik, G., Boris, J.P., Guirguis, R.H., and Oran, E.S., *J. Computational Physics*, 71: 1-20 (1987).
10. Oran, E.S., Boris, J.P., *Numerical Simulation of Reactive Flow*, Elsevier, New York, 1987.
11. Casulli, V., and Greenspan, D., *Int. J. Num. Methods Fluids* , 4:1001-1012 (1984).
12. Kee, R.J., Dixon-Lewis, G., Warnatz, J., Coltrin, M.E., and Miller, J.A., *A Fortran Computer Code Package for the Evaluation of Gas-Phase Multicomponent Transport Properties*, SAND86-8246, Sandia National Laboratory (1986).
13. Jones, W.W.and Boris, J.P., *Comp. and Chem.*, 5: 139-146 (1981).
14. Kailasanath, K., Oran, E.S., and Boris, J.P., "A One-Dimensional Time-Dependent Model for Flame Initiation, Propagation, and Quenching", NRL Memorandum Report 4910, Naval Research Laboratory (1982).
15. Bird, R.B., Stewart, W.E., and Lightfoot, E.N., *Transport Phenomema*, John Wiley and Sons, N.Y. (1960).

16. Wilke, C.R., *J. Chem. Phys.*, 18: 578-579 (1950).

17. Patnaik, G., Laskey, K.J., Kailasanath, K., Oran, E.S., and Brun, T.A., "FLIC–A Detailed, Two-Dimensional Flame Model," NRL Memorandum Report 6555, Naval Research Laboratory (1989).

18. Chamberlin, D.S., and Rose, A., *First Symposium on Combustion*, Sept. 10-14, 1928, Swampscott, MA, The Combustion Institute, Pittsburgh 1965 p. 27.

19. Kimura, I., *Tenth Symposium (International) on Combustion*, Aug. 17-21, 1964, Cambridge, England, The Combustion Institute, Pittsburgh 1965 p. 1295.

20. Ballantine, A. and Bray, K.N.C., *Sixteenth Symposium (International) on Combustion*, Aug. 15-20, 1976, Cambridge, MA, The Combustion Institute, Pittsburgh 1977 p. 777.

21. Chen, L.-D., Seaba, J.P., Roquemore, W.M., and Goss, L.P., *Twenty-Second Symposium (International) on Combustion*, Aug. 14-19, Seattle, WA, 1988, The Combustion Institute, Pittsburgh 1989 p. 677.

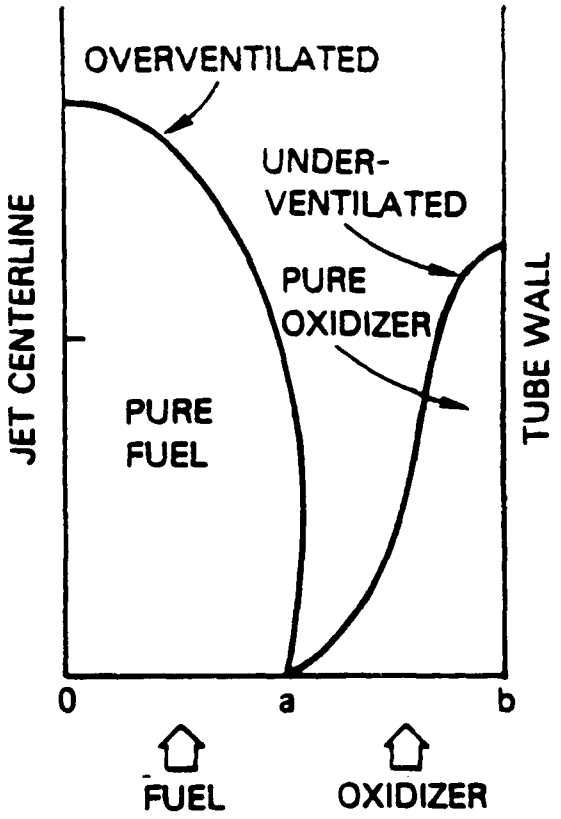

Fig. 1 — Geometry used for Burke-Schumann calculations showing flame location for typical underventilated or overventilated flame

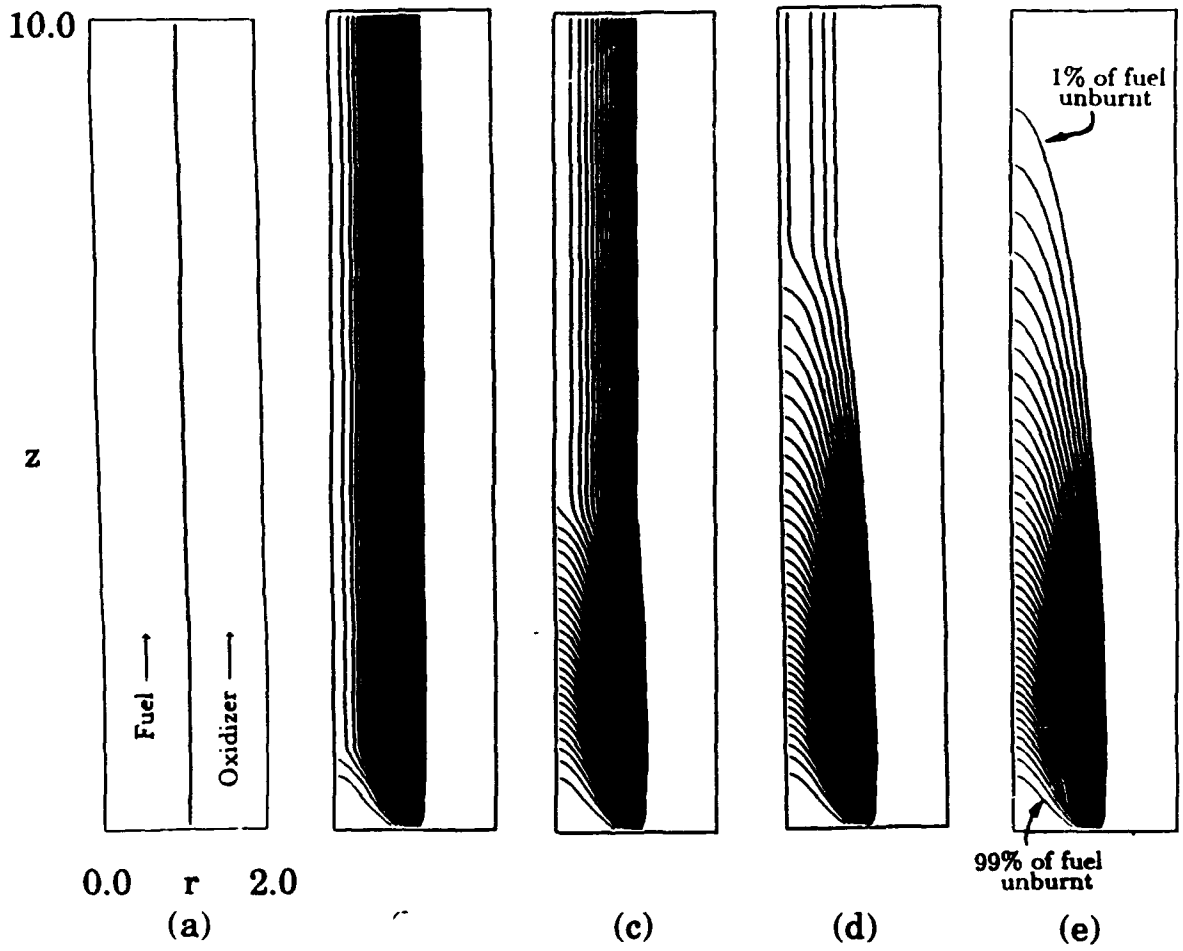

Fig. 2a — Contours of fuel concentration normalized by inlet fuel concentration for overventilated Burke-Schumann at times (a) 0.0 (b) 0.1 sec (c) 0.4 (e) 1.0 seconds

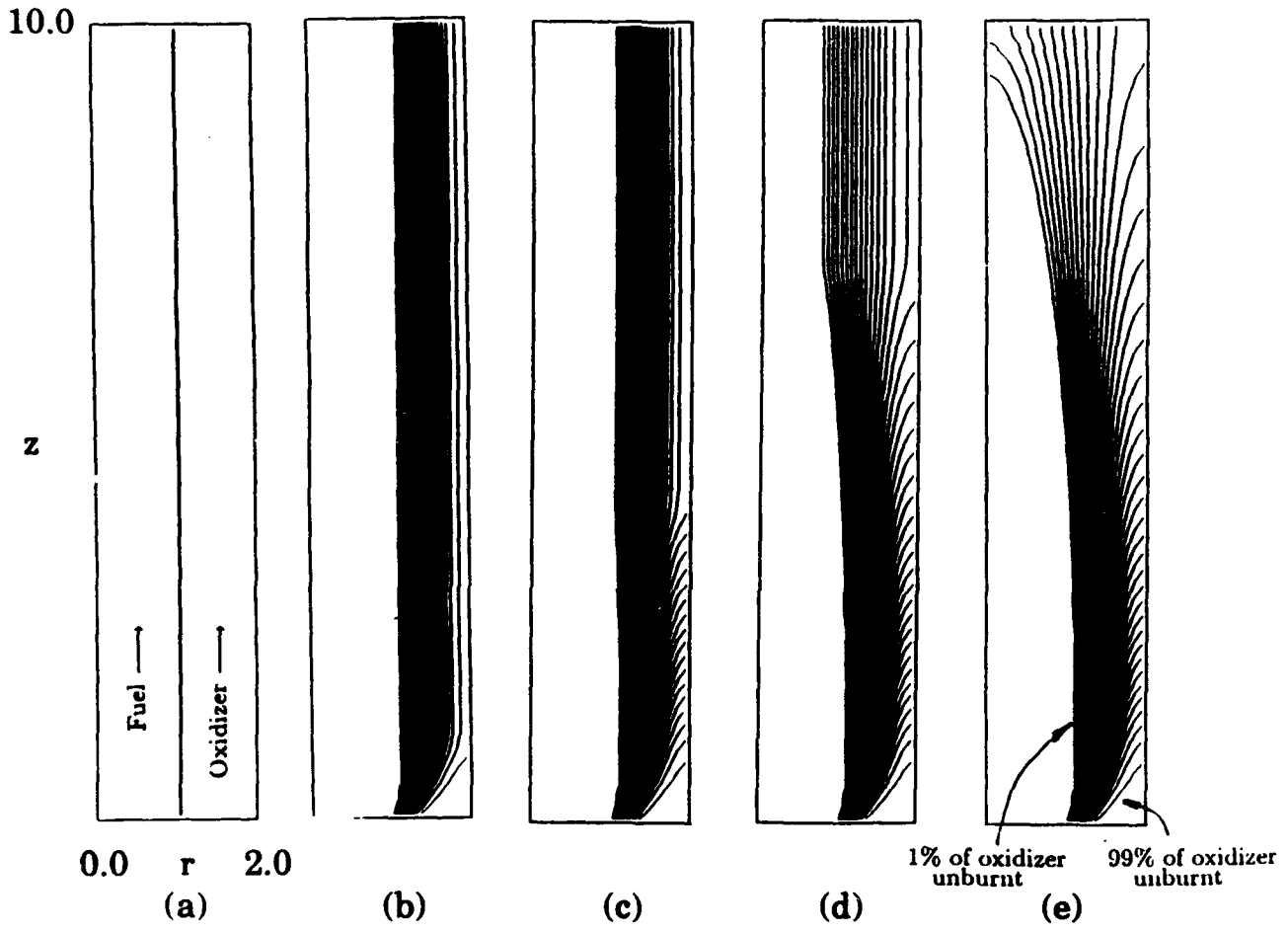

Fig. 2b — Contours of oxidizer concentration normalized by inlet oxidizer concentration for overventilated Burke-Schumann at times (a) 0.0 (b) 0.1 sec (c) 0.4 sec (d) 0.7 (e) 1.0 seconds

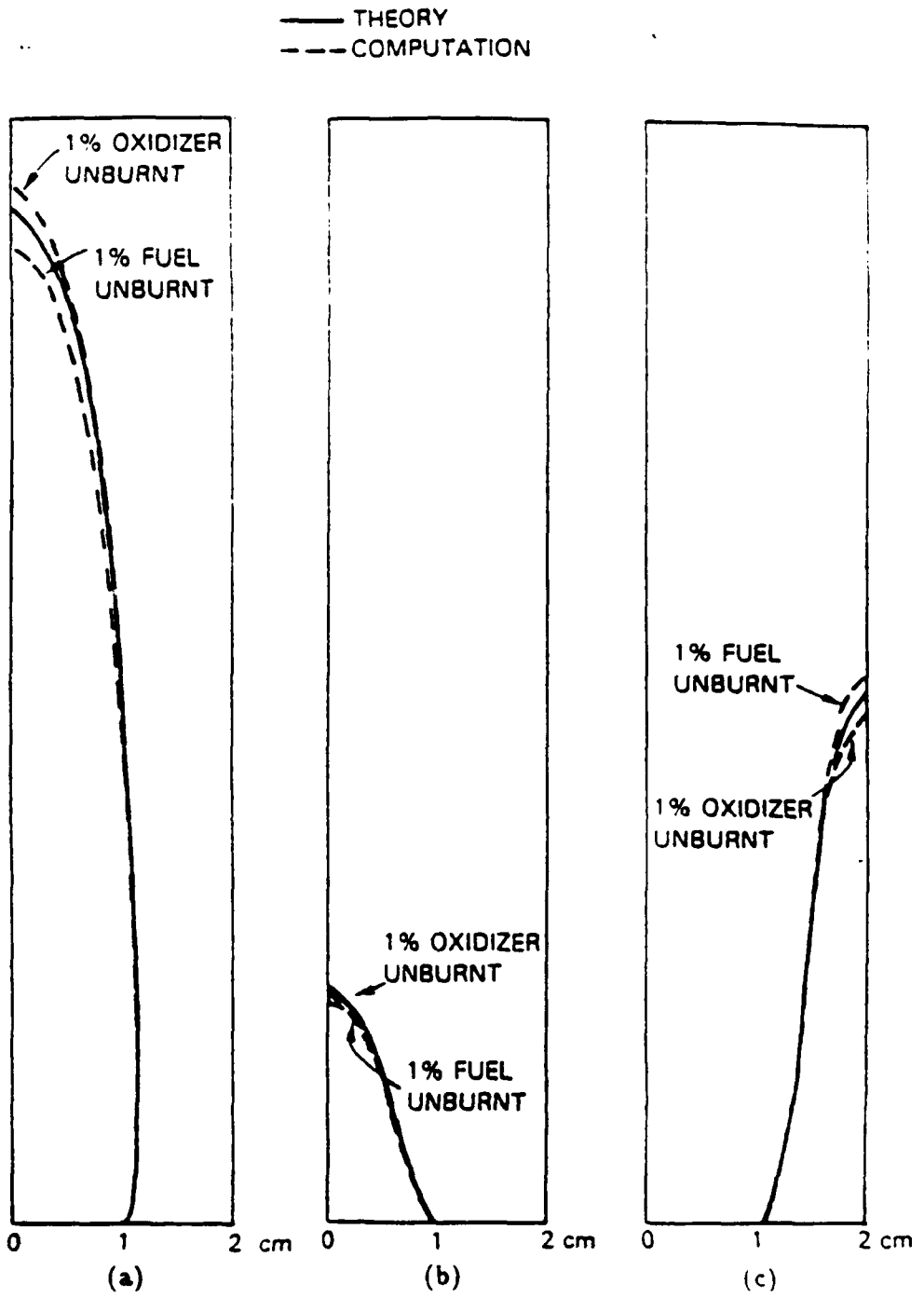

Fig. 3 — Comparison of analytical and computed solutions for flame location for three different Burke-Schumann flames. (a) Pure fuel reacting with 1 part oxidizer + 1 part inert. (b) One part fuel + 3 parts inert reacting with pure oxidizer. (c) Pure fuel reacting with 1 part oxidizer + 4 parts inert.

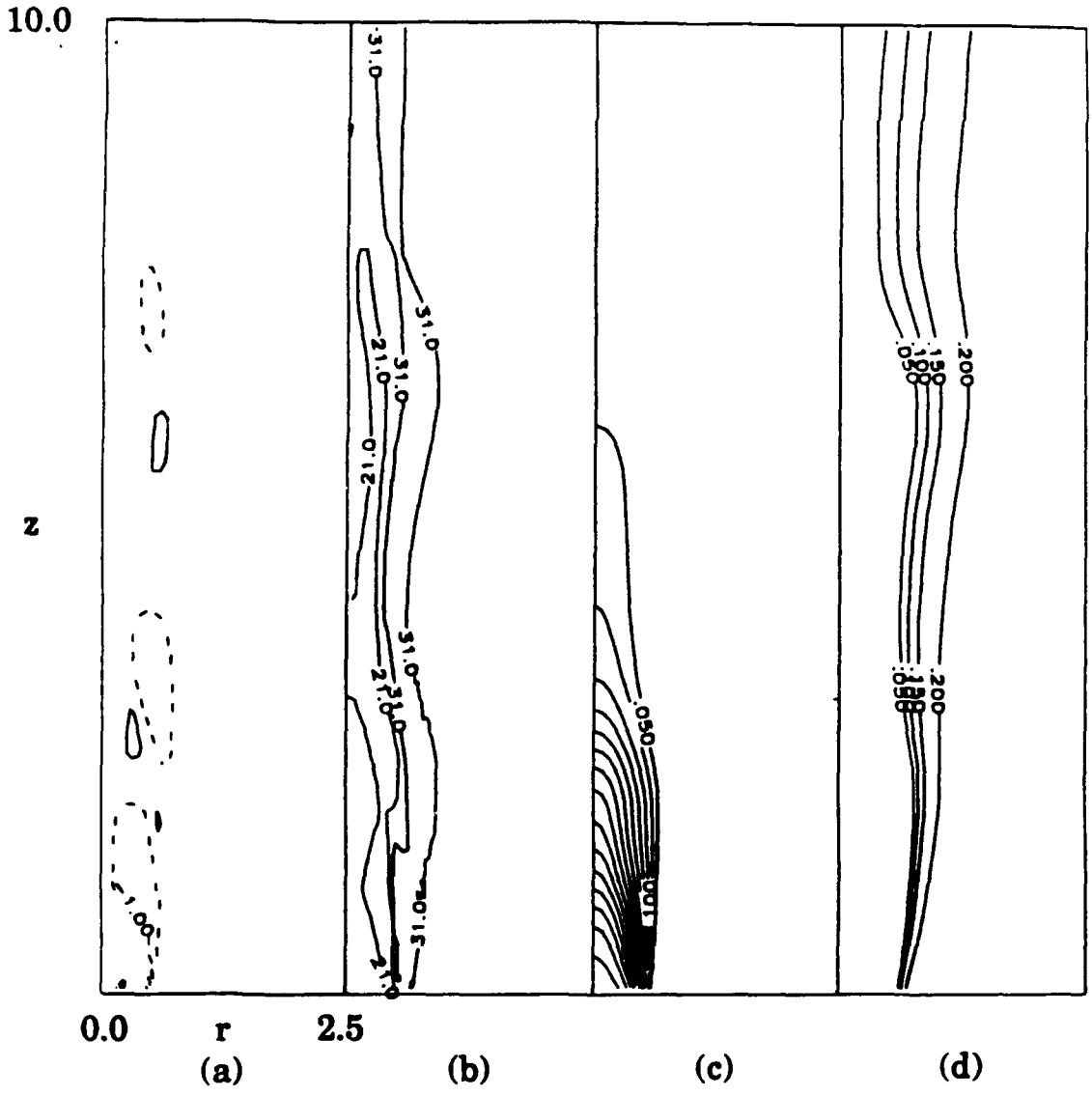

Fig. 4 — Contours of (a) radial velocity (b) axial velocity (c) mole fraction H_2 (d) mole fraction O_2 for $H_2 - N_2$ diffusion flame without heat release. Dimensions are in cm, velocities are in cm/s.

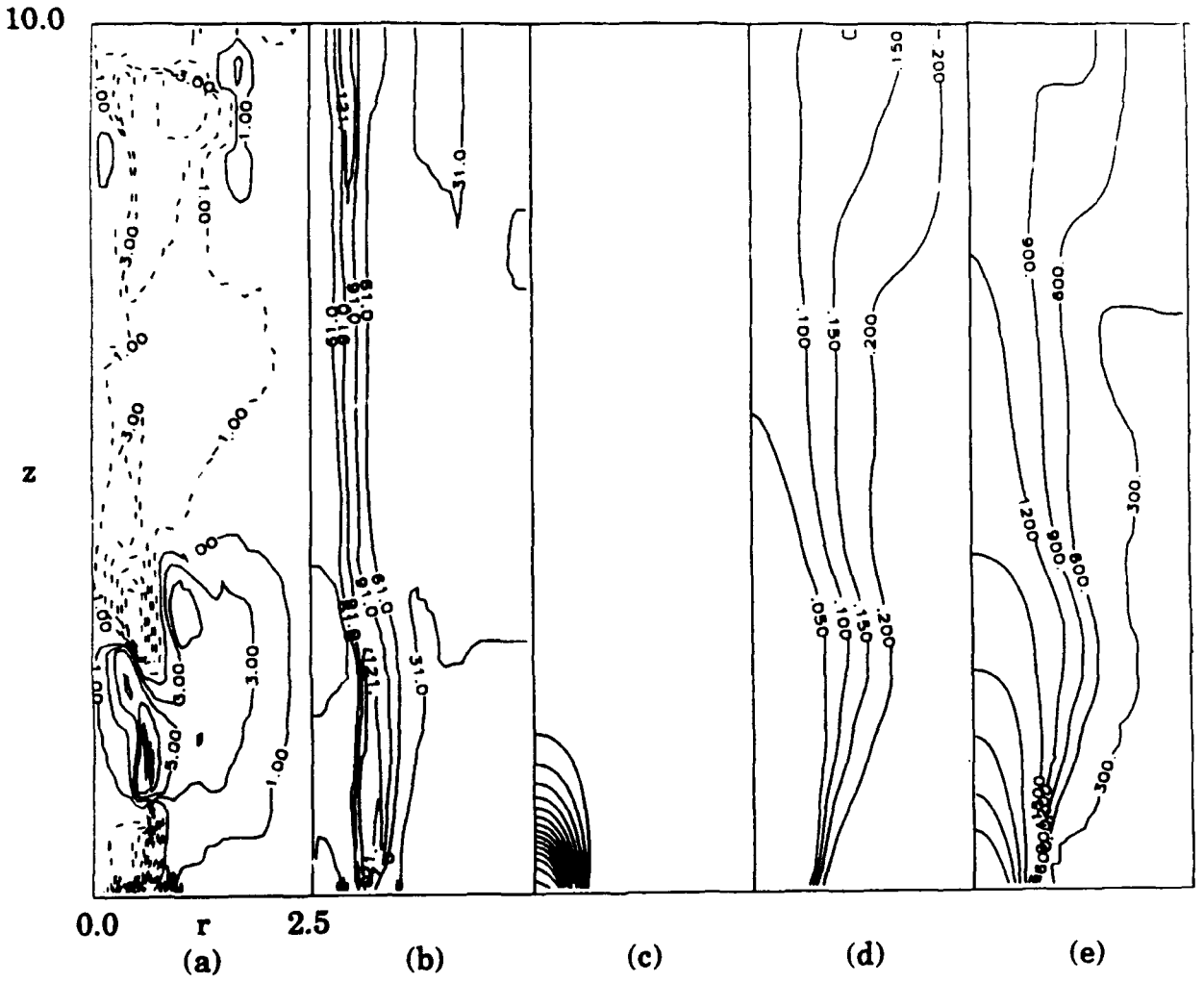

Fig. 5 — Contours of (a) radial velocity (b) axial velocity (c) mole fraction H_2 (d) mole fraction O_2 (e) temperature for $H_2 - N_2$ diffusion flame with heat release. Dimensions are in cm, velocities are in cm/s, temperature is in K.

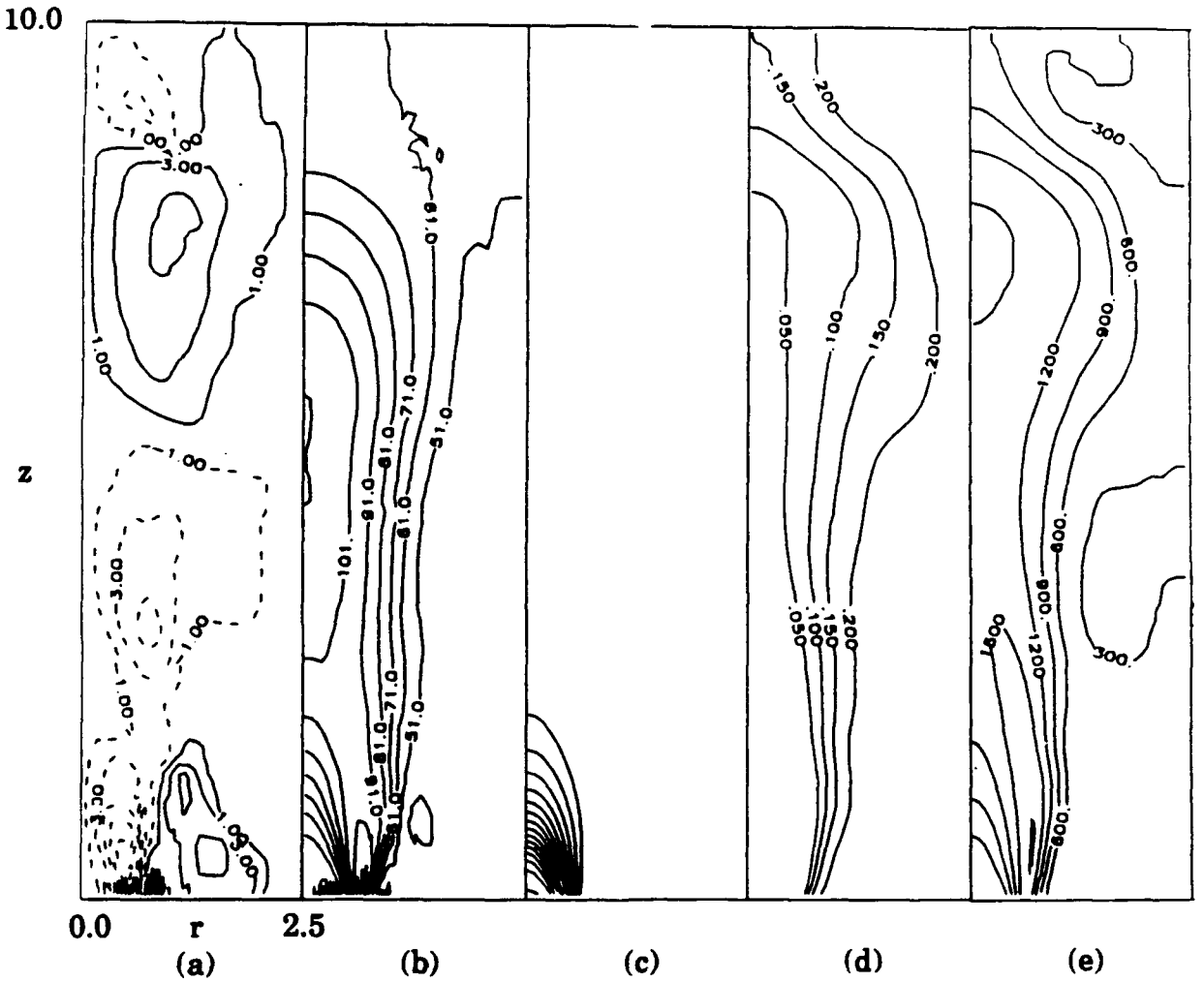

Fig. 6 — Contours of (a) radial velocity (b) axial velocity (c) mole fraction H_2 (d) mole fraction O_2 (e) temperature for $H_2 - N_2$ diffusion flame with heat release and viscosity. Dimensions are in cm, velocities are in cm/s, temperature is in K.

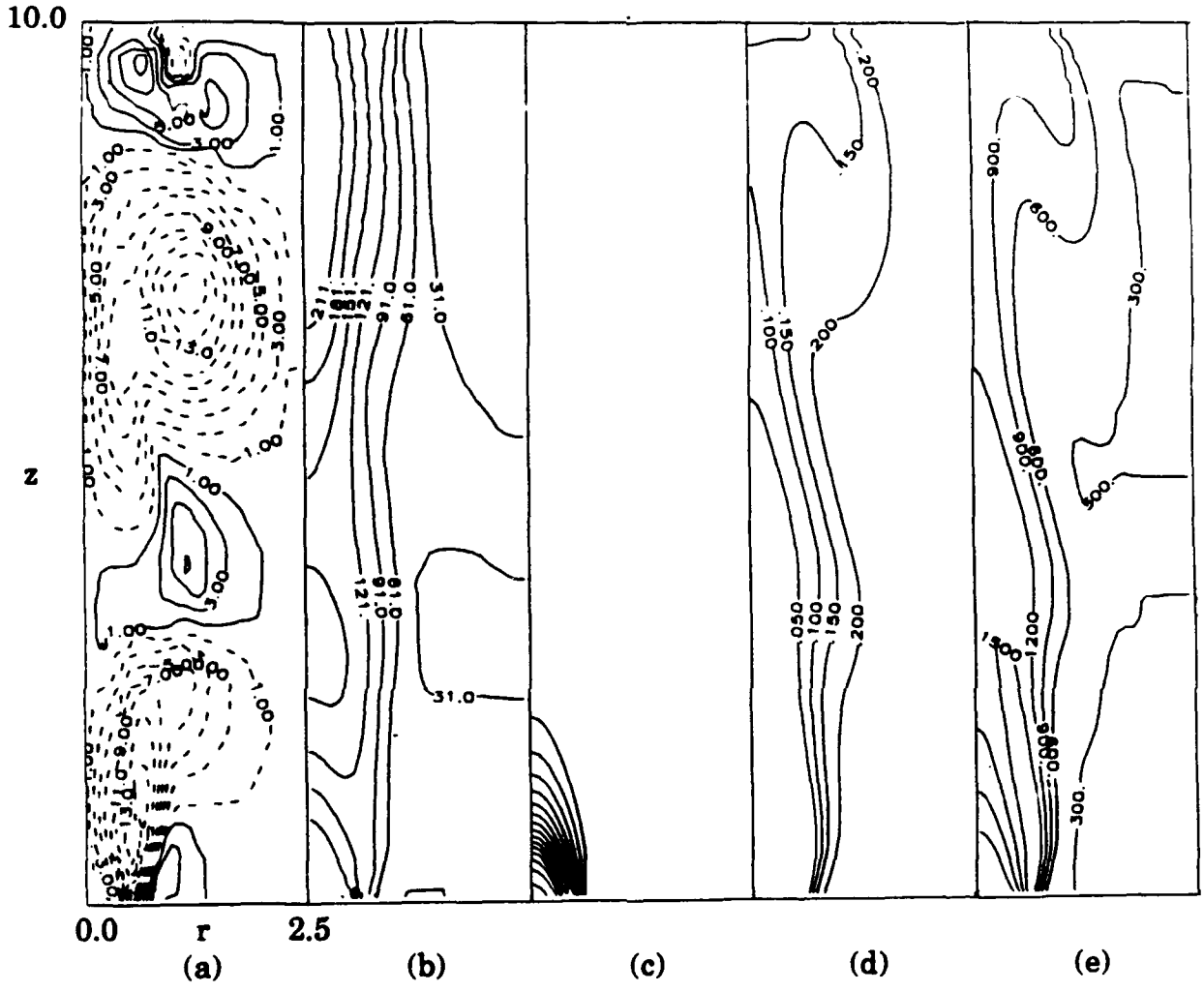

Fig. 7 — Contours of (a) radial velocity (b) axial velocity (c) mole fraction H_2 (d) mole fraction O_2 (e) temperature for $H_2 - N_2$ diffusion flame with heat release, viscosity, and gravity. Dimensions are in cm, velocities are in cm/s, temperature is in K.

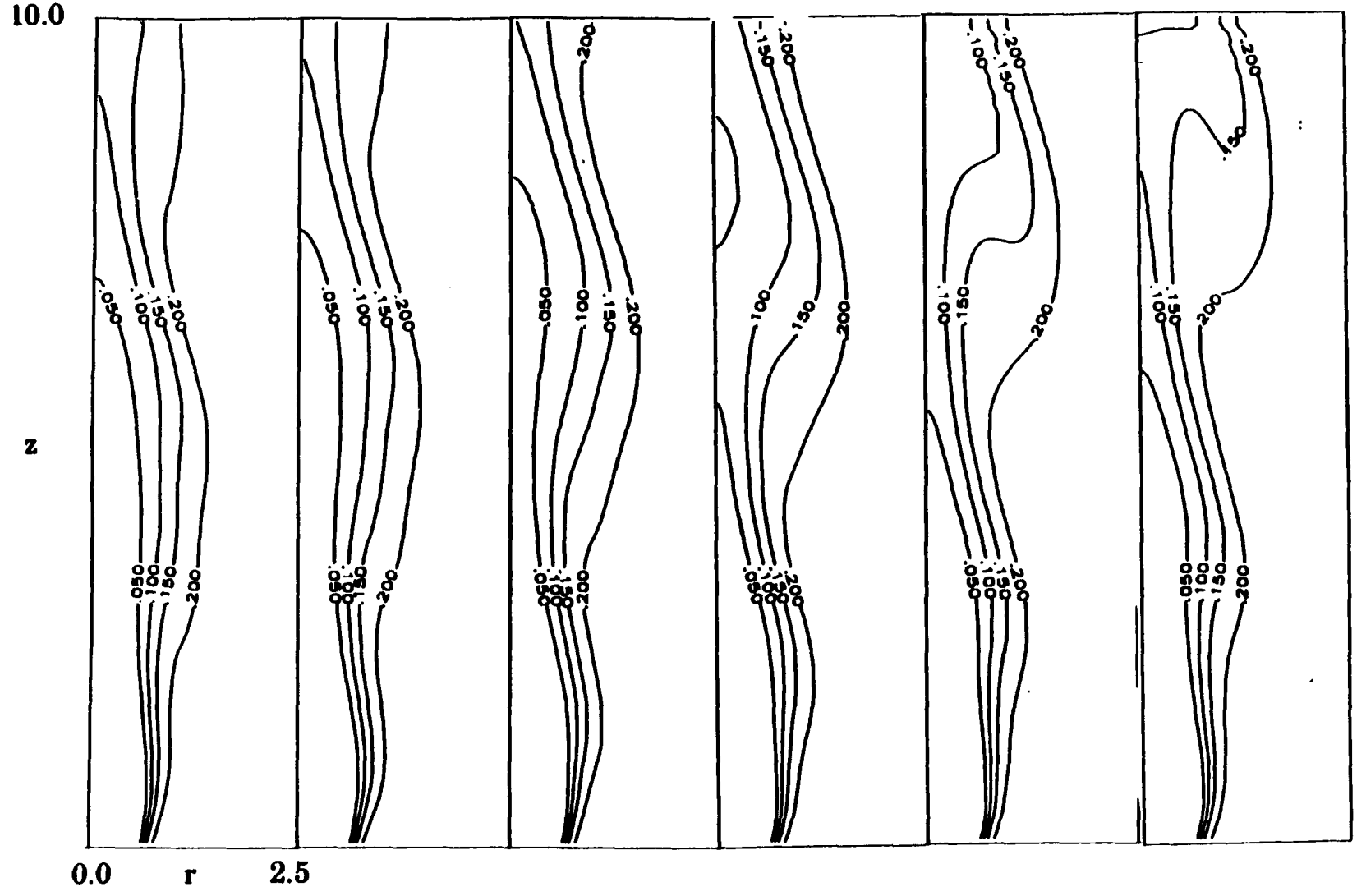

Fig. 8 — Time sequence for contours of O_2 mole fraction showing the formation of large structure. The time interval between each frame is 10 ms.